BIOMEDICAL ANALOG ELECTRONICS

Design and eSim Verification with Edge IoT Telemetry Integration of a Biopotential AFE

Enhanced Baseline Recovery, Ultra High Input Impedance and Interference Suppression

KiCad Schematics • Ngspice Simulation • Mathematical Modeling • ECG Analysis

Name	Sambuddha Samanta
Student ID	
Programme	B.Tech — Electrical Engineering (2nd Year, 3rd Sem)
Institution	Haldia Institute of Technology
Email	samantasambuddha9180@gmail.com
Project	ECG Analog Front-End Design and Simulation
Platform	eSim (FOSSEE, IIT Bombay) with ngspice
Date	August 2026

Circuit-level modeling, comparative simulation and performance evaluation of ECG acquisition architectures.

Contents

1 Abstract

Capacitive biopotential measurements (CBMs) are getting popular for long-term and non-contact ECG monitoring, but their high input-impedance requirement can cause slow baseline recovery and higher sensitivity to stray capacitance. In this work, I have designed and simulated an ECG analog front end using a dynamic Bootstrapped Non-Inverting Amplifier (BNA) stage with voltage-dependent resistance, bandpass amplification and stray capacitance compensation.

For the stray-capacitance test, I used a total input capacitance of 330 pF with a 30 pF compensation capacitor. The ECG peak-to-peak amplitude improved by **12.34%** at the input and **12.49%** at the BNA output. For the recovery test, the nonlinear resistance reduced to about 44.07 kΩ and the measured baseline-recovery time was 30.07 s.

I have tried to implement a complete IoT system through analog filtering, an 8-bit ADC at 250 S/s, QRS detection and OOK telemetry. Using a recorded PTB-XL ECG, the system detected **8 cardiac events**, estimated a heart rate of about 50.85 bpm, and recovered all **8/8 events** after transmission.

Overall, the simulation shows that the BNA-based AFE can maintain high input impedance during normal ECG acquisition while also helping with disturbance recovery and stray-capacitance effects.

The complete system was evaluated as a single transient circuit-level simulation in KiCad/eSim using ngspice and an OPA827 macromodel.

2 Introduction and Theoretical Background

Electrocardiography measures the electrical activity of the heart through electrodes placed on the body surface. Since the useful ECG signal is small compared with many disturbances present at the electrode interface, the analog front-end must provide high input impedance, differential amplification, controlled bandwidth, and suppression of unwanted interference without significantly altering ECG morphology.

2.1 ECG Acquisition Challenges

Several mechanisms degrade the acquired signal. Motion of the electrode and variations in the electrode–skin interface can produce large low-frequency transients and baseline displacement. Environmental electric fields may couple common-mode interference into the body and measurement leads, while mains interference can appear around the power-line frequency.

Parasitic capacitance between the amplifier input, surrounding conductors, PCB structures, and ground also affects signal transfer. When combined with a large electrode or source impedance, this capacitance forms an RC network that can attenuate higher-frequency ECG components.

Front-End Design Requirement

The proposed front-end must simultaneously:

- maintain very high input impedance during normal ECG acquisition;
- reduce its effective discharge impedance during large disturbances;
- limit parasitic-capacitance loading at the BNA input.

2.2 Input Impedance and Baseline Recovery

A high input resistance minimizes current drawn from the electrode interface. However, when a large transient charges an input capacitance, the discharge behaviour is governed approximately by

$$\tau = RC. \tag{1}$$

A fixed high-resistance front-end may therefore provide excellent sensitivity during normal operation while exhibiting slow recovery after a large disturbance.

The proposed BNA addresses this trade-off using a nonlinear resistance. During normal ECG acquisition it remains close to its high-resistance state. Once the disturbance exceeds the switching region, the resistance falls and creates a temporary discharge path. As the disturbance decays, the high-resistance state is restored.

2.3 Parasitic Input Capacitance

For a source resistance R_{src} and input stray capacitance C_{st}, the approximate RC corner is

$$f_c \approx \frac{1}{2\pi R_{\text{src}} C_{st}}. \tag{2}$$

At very high source impedance, even picofarad-level capacitance can influence signal transfer. The BNA therefore incorporates capacitive neutralization using a compensation capacitor C_n, analyzed in detail in Section 6.

2.4 Analog Conditioning and Edge Processing

Following the two BNA channels, the ECG is differentially amplified and passed through notch, low-pass, and high-pass filtering. The final analog signal is AC-coupled, shifted around the midpoint of a 0 V to 3.3 V ADC range, sampled at 250 S/s, and quantized to 8-bit resolution.

The edge-processing section then extracts QRS events and generates one event pulse per detected heartbeat. These pulses control an on–off-keyed telemetry carrier, while the receiver reconstructs the event sequence using rectification, envelope detection, and threshold logic.

3 System Architecture and Signal Flow

The complete system combines the adaptive analog front-end, ADC interface, QRS-event extraction, and telemetry chain within one integrated transient simulation.

3.1 Proposed Architecture

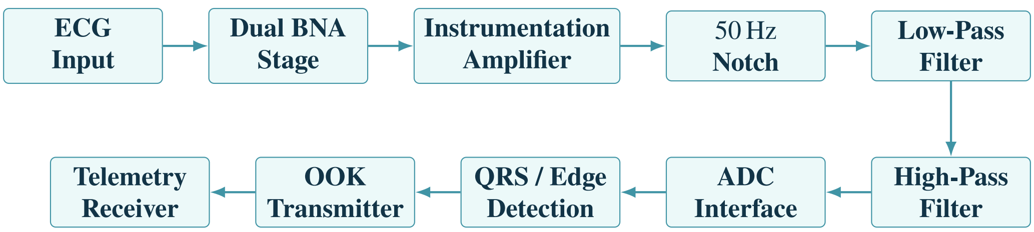

Figure 1: Integrated ECG analog front-end and edge-telemetry architecture.

3.2 Signal-Flow Description

Table 1 summarizes the progression of the ECG through the complete system.

Table 1: Signal flow through the integrated ECG acquisition system.

Stage	Principal Node(s)	Function	Output
ECG Source	`body_p`, `body_n`	Generates the differential ECG excitation.	Differential ECG
BNA Input	`v2`, `v3`	Provides high input impedance, adaptive recovery and parasitic compensation.	Protected inputs
BNA Output	`vout1`, `vout2`	Buffers and conditions the two acquisition channels.	Dual BNA outputs
Instrumentation Amplifier	`vnotchin`	Amplifies the differential ECG component.	Amplified ECG
Notch Filter	`vnotchout`	Suppresses interference around 50 Hz.	Notch output
Low-Pass Filter	`vlopout`	Restricts excessive high-frequency content.	LPF output
High-Pass Filter	`vhpout`	Suppresses very-low-frequency baseline components.	Final AFE output
ADC Interface	`adc_ac`, `adc_in`	Removes DC, applies gain, and rebiases around 1.65 V.	ADC-ready ECG
Sampling / Quantization	`adc_hold`, `adc_quant`	Samples at 250 S/s and performs 8-bit quantization.	Quantized ECG
QRS Detection	`qrs_env`, `event_pulse`	Extracts cardiac events using threshold and refractory logic.	Beat events
OOK Transmitter	`tx_ook`	Gates the telemetry carrier using detected events.	OOK waveform
Channel	`rx_raw`	Introduces attenuation and channel interference.	Received waveform
Receiver	`event_rx`	Recovers cardiac events from the received envelope.	Recovered events

3.3 Principal Design Parameters

Table 2: Principal system-level design parameters.

Parameter	Value
BNA bias resistance	100 MΩ
Maximum nonlinear resistance	20 MΩ
BNA feedback network	$R_f = 270\,\mathrm{k\Omega},\ C_f = 5.7\,\mathrm{nF}$
BNA series network	$R_s = 30\,\mathrm{k\Omega},\ C_s = 10.7\,\mathrm{\mu F}$
Final stray capacitance	15 pF
Final neutralization capacitance	1 pF
Recovery coupling capacitance	10 nF
Precharge magnitude	3.2 V
ADC range	0 V to 3.3 V
ADC resolution	8 bit
Sampling rate	250 S/s
Telemetry carrier	100 Hz
Channel attenuation	0.35
Channel interference	23 Hz, 30 mV

4 Design and Simulation Methodology

The complete circuit was developed in KiCad/eSim and simulated using ngspice. OPA827 operational-amplifier macromodels were used throughout the active analog stages so that input conditioning, differential amplification, filtering, digitization, event extraction, and telemetry could be evaluated within one circuit-level simulation.

4.1 ECG Input Model

A recorded ECG waveform was converted to a piecewise-linear voltage source and applied differentially to the two body nodes:

$$V_{body,p} = +\frac{1}{2}V_{\text{ECG}}, \quad (3)$$
$$V_{body,n} = -\frac{1}{2}V_{\text{ECG}}. \quad (4)$$

This arrangement preserves the differential ECG while allowing controlled source impedance, stray capacitance, and transient disturbances to be introduced at the BNA input.

4.2 Transient Simulation Strategy

Different intervals of the same transient simulation are reserved for the individual evaluations summarized in Table 3.

Table 3: Transient-analysis intervals used in the integrated simulation.

Test	Interval	Purpose
Stray capacitance, C_n OFF	0–9.99 s	Reference ECG under intentional capacitive loading.
Stray capacitance, C_n ON	9.99–19.98 s	A/B evaluation of capacitive neutralization.
Final AFE settling	19.99–30 s	Restoration of final C_{st} and C_n.
Baseline disturbance	approximately 30 s onward	Dynamic BNA switching and baseline-recovery evaluation.
Final system evaluation	90–101.8 s	AFE, ADC, QRS and telemetry measurements.

4.3 Measurement Method

Performance quantities were extracted directly from the ngspice transient solution using automated `.meas` statements. Peak-to-peak amplitude, RMS value, switching times, steady-state baseline, ADC range, event timing, RR interval, heart rate, and telemetry delay were therefore obtained from the same transient solution used for waveform inspection.

Simulation Strategy
The report emphasizes transient circuit behaviour rather than separate AC-sweep verification. Frequency limits associated with the BNA are derived analytically from the component values, while the principal performance claims are obtained from the integrated transient simulation.

5 Dynamic BNA Input Stage

The proposed analog front-end begins with two matched Boot Strapped Non-Inverting Amplifier (BNA) channels connected to the positive and negative ECG inputs. The BNA performs three principal functions:

1. Preservation of very high input impedance during normal ECG acquisition;
2. Pemporary reduction of discharge impedance during large electrode disturbances;

3. Reduction of the effect of input stray capacitance through capacitive neutralization.
4. Bandpass amplification allowing only necessary signals to pass and amplify

The positive channel processes node v_2 and generates v_{out1}, while the negative channel processes v_3 and generates v_{out2}. Both channels use the same BNA structure and component values.

5.1 BNA Circuit Topology

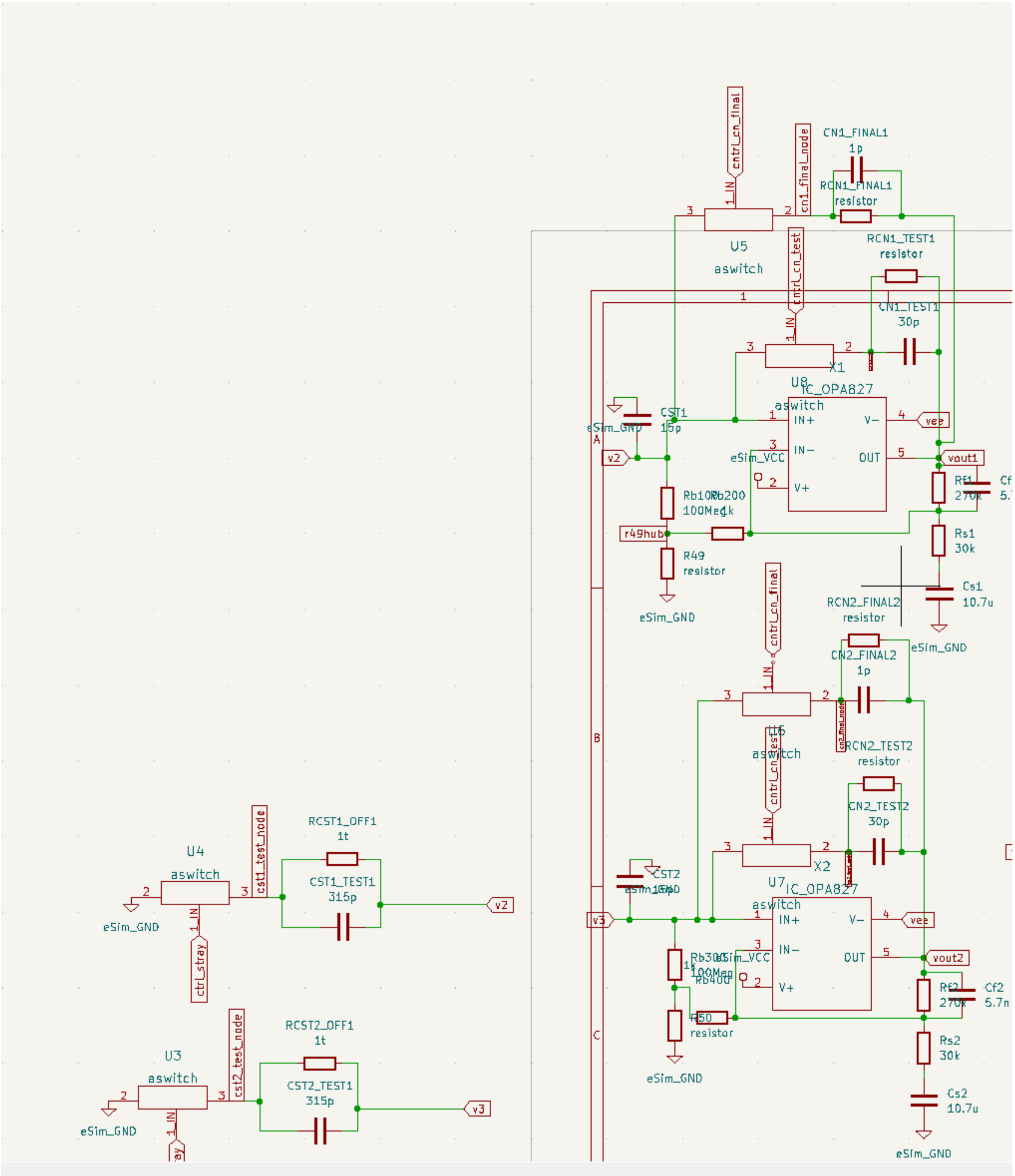

Figure 2: Dual-channel BNA input stage used in the integrated AFE.

The principal component values of each BNA channel are

$$
\begin{aligned}
R_B &= 100\,\mathrm{M\Omega}, & R_f &= 270\,\mathrm{k\Omega}, & (5)\\
R_s &= 30\,\mathrm{k\Omega}, & C_f &= 5.7\,\mathrm{nF}, & (6)\\
C_s &= 10.7\,\mu\mathrm{F}. & & & (7)
\end{aligned}
$$

The 100 MΩ resistance provides the high impedance input path, while the OPA827 and the $R_f - C_f$ and $R_s - C_s$ networks establish the active BNA behaviour.

Each channel also contains a nonlinear resistance, denoted R_{49} and R_{50}, whose value changes with the magnitude of the associated input-node voltage.

5.2 Permanent Input Stray Capacitance

An important part of the physical input model is the permanent capacitance

$$\boxed{C_{st,\mathrm{final}} = 15\,\mathrm{pF}}$$

connected between each BNA input and ground.

For the positive channel,

$$v_2 \longrightarrow C_{st1} = 15\,\mathrm{pF} \longrightarrow \mathrm{GND},$$

while the negative channel contains the identical connection at v_3.

Physical Meaning of C_{st}

The 15 pF capacitance represents the unavoidable parasitic capacitance associated with the amplifier input, PCB tracks, surrounding conductors, electrode wiring, and the electrical environment.
It is therefore part of the final AFE model and remains connected throughout normal ECG acquisition and baseline-recovery operation.

5.3 Voltage-Dependent BNA Resistance

The nonlinear resistance used in the positive BNA is represented by

$$R_{49}(V) = 20\,\mathrm{M\Omega} - (20\,\mathrm{M\Omega} - 1\,\mathrm{m\Omega})\,\frac{1 + \tanh\left[100\left(|V_{R49}| - V_{\mathrm{THR}}\right)\right]}{2}. \qquad (8)$$

The same relation is used for R_{50}.

For the selected configuration,

$$\boxed{V_{\mathrm{THR}} = 2.17\,\mathrm{V}}$$

The three important operating regions are summarized in Table 4.

Table 4: Operating regions of the nonlinear BNA resistance.

Condition	Approximate R_{49}	BNA State
$\lvert V_{R49}\rvert \ll V_{\mathrm{THR}}$	$20\,\mathrm{M\Omega}$	High-impedance ECG acquisition.
$\lvert V_{R49}\rvert = V_{\mathrm{THR}}$	$10\,\mathrm{M\Omega}$	Center of nonlinear transition.
$\lvert V_{R49}\rvert > V_{\mathrm{THR}}$	Strongly reduced	Large-disturbance discharge state.

Adaptive BNA Operation

Under normal conditions,

$$\lvert V_{R49}\rvert < V_{\mathrm{THR}}$$

and the resistance remains near

$$\boxed{R_{49} \approx 20\,\mathrm{M\Omega}}.$$

When the disturbance exceeds the threshold,

$$\lvert V_{R49}\rvert > V_{\mathrm{THR}},$$

the resistance falls sharply, creating a temporary lower-impedance discharge path. As the disturbance decays, the resistance automatically returns toward its high-resistance state.

5.4 Intrinsic BNA Frequency Range

The approximate lower-frequency limit is associated with R_s and C_s:

$$f_L \approx \frac{1}{2\pi R_s C_s} = \frac{1}{2\pi(30\,\mathrm{k\Omega})(10.7\,\mu\mathrm{F})} \approx \boxed{0.496\,\mathrm{Hz}}. \tag{9}$$

The approximate upper-frequency limit is associated with R_f and C_f:

$$f_H \approx \frac{1}{2\pi R_f C_f} = \frac{1}{2\pi(270\,\mathrm{k\Omega})(5.7\,\mathrm{nF})} \approx \boxed{103.4\,\mathrm{Hz}}. \tag{10}$$

Hence,

$$\boxed{0.50\,\mathrm{Hz} \lesssim f \lesssim 103.4\,\mathrm{Hz}}$$

represents the approximate intrinsic BNA operating range before the dedicated filtering stages.

5.5 Switch-Controlled Test Network

Voltage-controlled switches are used so that all characterization can be performed inside the same integrated transient simulation rather than using separate circuit files.

The switches themselves do not perform the capacitance compensation or baseline recovery. They only connect or disconnect the required test branches.

5.5.1 Temporary $50\,\mathrm{M\Omega}$ Source Path

During stray-capacitance characterization, the ECG is connected to the BNA through

$$\boxed{R_{\mathrm{src}} = 50\,\mathrm{M\Omega}}.$$

Thus,

$$body_p \longrightarrow 50\,\mathrm{M\Omega} \longrightarrow v_2$$

and similarly for the negative channel.

A finite source resistance is necessary because an ideal voltage source would force the voltage at v_2 and largely conceal the loading effect of C_{st}.

5.5.2 Temporary Additional Stray Capacitance

The permanent input capacitance is always

$$C_{st,\mathrm{final}} = 15\,\mathrm{pF}.$$

For the A/B stress test, an additional switched capacitor

$$C_{st,\mathrm{extra}} = 315\,\mathrm{pF}$$

is placed from the BNA input toward ground.

While its switch is closed,

$$C_{st,\mathrm{total}} = 15\,\mathrm{pF} + 315\,\mathrm{pF} = \boxed{330\,\mathrm{pF}}.$$

When the switch opens, only the permanent

$$\boxed{15\,\mathrm{pF}}$$

remains.

5.5.3 Floating-Node Protection

When the temporary capacitor is disconnected, its intermediate node would be connected only through a capacitor and would have no defined DC path.

A very large resistor,

$$\boxed{R_{\mathrm{OFF}} = 1\,\mathrm{T\Omega}}$$

is therefore included to provide a weak DC reference.

Its resistance is sufficiently large to have negligible influence on normal signal operation while preventing a completely floating SPICE node.

5.5.4 Compensation-Capacitor Switching

Two neutralization capacitors are used:

$$\boxed{C_{n,\mathrm{test}} = 30\,\mathrm{pF}}$$

for the A/B characterization, and

$$\boxed{C_{n,\mathrm{final}} = 1\,\mathrm{pF}}$$

for final normal AFE operation.

Separate switch nodes are used so that the two capacitors can be connected independently.

Table 5: Switch-controlled BNA test configuration.

Controlled Branch	Active Interval	Function
50 MΩ **source path**	0–19.98 s	Finite source impedance for C_{st} testing.
Additional 315 pF C_{st}	0–19.98 s	Produces the controlled 330 pF stress condition.
30 pF C_n	9.99–19.98 s	Compensation ON during second ECG cycle.
Final 1 pF C_n	19.99 s onward	Final BNA neutralization network.
Precharge network	until approximately 29.99 s	Stores the controlled recovery disturbance.
Electrode contact	from approximately 30.01 s	Applies the stored disturbance to the BNA.

6 Stray-Capacitance Compensation

The capacitive-neutralization capability of the BNA is evaluated using a controlled A/B transient experiment. The same recorded ECG waveform is applied under identical source conditions first without compensation and subsequently with compensation enabled.

6.1 Selection of the Stress Capacitance

The permanent parasitic capacitance is

$$C_{st,\text{final}} = 15\,\text{pF}.$$

However, this small capacitance produces only a subtle effect on the millivolt-level ECG waveform. A larger temporary capacitance is therefore used to provide a measurable stress condition.

The test value is not selected arbitrarily. The BNA neutralization condition is approximately

$$\boxed{C_n < \frac{R_s}{R_f} C_{st}} \tag{11}$$

or equivalently,

$$\boxed{C_{st} > \frac{R_f}{R_s} C_n}. \tag{12}$$

For $R_f = 270\,\text{k}\Omega$ and $R_s = 30\,\text{k}\Omega$, the gain ratio is $R_f/R_s = 9$.
A convenient test compensation capacitor of $\boxed{C_{n,\text{test}} = 30\,\text{pF}}$ therefore requires $C_{st} > 9 \times 30\,\text{pF}$, or

$$\boxed{\mathbf{C_{st}} > 270\,\text{pF}}$$

A total stress capacitance of $\boxed{C_{st,\text{stress}} = 330\,\text{pF}}$ was selected to remain safely above this minimum while producing a readily observable input-loading effect.

Since 15 pF is already permanently present, the required additional capacitor is

$$C_{st,\text{extra}} = C_{st,\text{stress}} - C_{st,\text{final}} \tag{13}$$
$$= 330\,\text{pF} - 15\,\text{pF} \tag{14}$$
$$= \boxed{315\,\text{pF}}. \tag{15}$$

Why 330 pF and 30 pF?

The pair is deliberately selected so that

$$\boxed{C_n < \frac{R_s}{R_f} C_{st}}$$

remains satisfied:

$$30\,\text{pF} < \frac{30}{270}(330\,\text{pF}) = 36.67\,\text{pF}.$$

Thus,

$$\boxed{30\,\text{pF} < 36.67\,\text{pF}}$$

provides a compensated but non-overcompensated stress condition.

6.2 Uncompensated RC Loading

With the temporary source resistance $\boxed{R_{\text{src}} = 50\,\text{M}\Omega}$ and the stressed capacitance $\boxed{C_{st} = 330\,\text{pF}}$, the approximate RC corner frequency is

$$\boxed{f_{c,\text{stress}} = \frac{1}{2\pi(50\,\text{M}\Omega)(330\,\text{pF})} \approx 9.65\,\text{Hz}}$$

The comparatively low corner frequency of 9.65 Hz makes the capacitive loading clearly visible in the ECG waveform during the stress test.

$$f_{c,\text{stress}} = \frac{1}{2\pi R_{\text{src}} C_{st}} \tag{16}$$
$$= \frac{1}{2\pi(50\,\text{M}\Omega)(330\,\text{pF})} \tag{17}$$
$$\approx \boxed{9.65\,\text{Hz}}. \tag{18}$$

The comparatively low corner frequency attenuates the sharper ECG components, making the effect of the input capacitance clearly observable.

6.3 Neutralization Principle

The feedback capacitor C_n produces an approximate negative-capacitance contribution at the input:

$$\boxed{C_{\text{neg}} \approx -\frac{R_f}{R_s} C_n} \tag{19}$$

For the test compensation capacitor $\boxed{C_n = 30\,\text{pF}}$, the effective negative-capacitance contribution is

$$\boxed{C_{\text{neg}} \approx -\frac{270}{30}(30\,\text{pF}) = -9(30\,\text{pF}) = -270\,\text{pF}}$$

Therefore, with the stressed physical capacitance $\boxed{C_{st} = 330\,\text{pF}}$, the approximate residual effective capacitance becomes

$$\boxed{C_{\text{eff}} \approx C_{st} + C_{\text{neg}} = 330\,\text{pF} - 270\,\text{pF} = 60\,\text{pF}}$$

Thus, the physical 330 pF capacitance remains connected, while the active neutralization network reduces the effective capacitive loading seen by the ECG source to approximately 60 pF.

$$\begin{aligned} C_{\text{eff}} &\approx C_{st} + C_{\text{neg}} && (20) \\ &= 330\,\text{pF} - 270\,\text{pF} && (21) \\ &= \boxed{60\,\text{pF}}. && (22) \end{aligned}$$

The corresponding approximate compensated RC corner becomes

$$\begin{aligned} f_{c,\text{comp}} &\approx \frac{1}{2\pi(50\,\text{M}\Omega)(60\,\text{pF})} && (23) \\ &\approx \boxed{53.1\,\text{Hz}}. && (24) \end{aligned}$$

Thus the compensation changes the approximate loading corner from

$$\boxed{9.65\,\text{Hz} \longrightarrow 53.1\,\text{Hz}}$$

under the controlled stress condition.

6.4 A/B Test Sequence

Table 6: Capacitive-neutralization A/B test sequence.

Interval	Total C_{st}	C_n	Condition
0–9.99 s	330 pF	OFF	Uncompensated stress reference.
9.99–19.98 s	330 pF	30 pF	Compensated stress condition.
19.99 s onward	15 pF	1 pF	Final BNA configuration.

6.5 BNA-Output Comparison

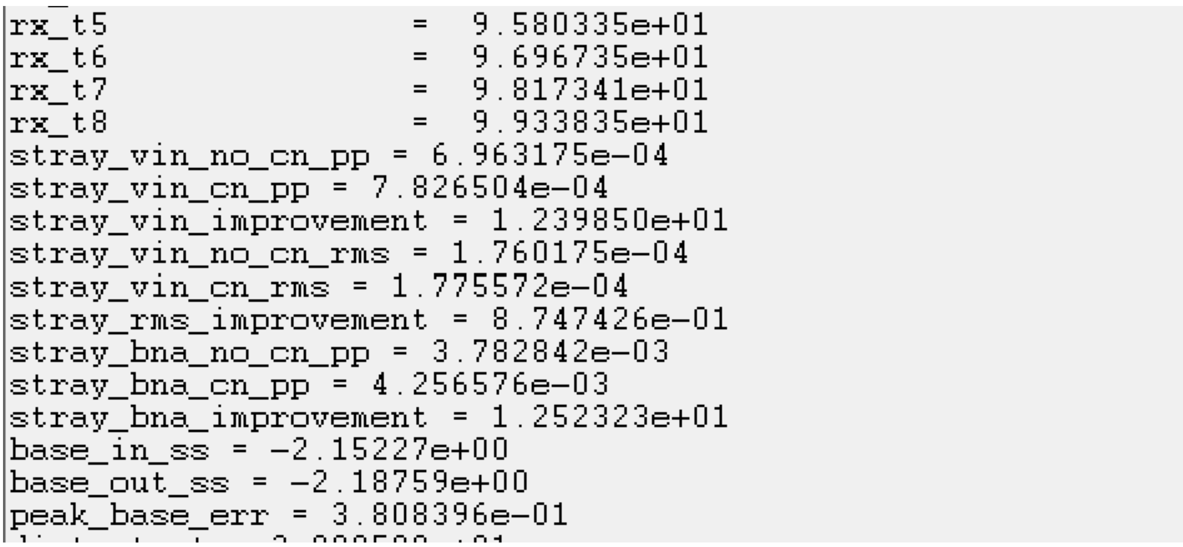
```
rx_t5                   =  9.580335e+01
rx_t6                   =  9.696735e+01
rx_t7                   =  9.817341e+01
rx_t8                   =  9.933835e+01
stray_vin_no_cn_pp = 6.963175e-04
stray_vin_cn_pp = 7.826504e-04
stray_vin_improvement = 1.239850e+01
stray_vin_no_cn_rms = 1.760175e-04
stray_vin_cn_rms = 1.775572e-04
stray_rms_improvement = 8.747426e-01
stray_bna_no_cn_pp = 3.782842e-03
stray_bna_cn_pp = 4.256576e-03
stray_bna_improvement = 1.252323e+01
base_in_ss = -2.15227e+00
base_out_ss = -2.18759e+00
peak_base_err = 3.808396e-01
```

Figure 3: Different parameter comparisons during the stray-capacitance A/B test.

6.6 Measured Compensation Performance

Table 7: Measured effect of capacitive neutralization.

Quantity	Compensation OFF	Compensation ON	Improvement
Input ECG V_{pp}	0.6963 mV	0.7826 mV	**12.34%**
BNA output V_{pp}	3.782 mV	4.256 mV	**12.49%**
Input ECG RMS	0.1760 mV	0.1775 mV	**0.88%**

6.7 Final BNA Capacitance Configuration

Final BNA Capacitance Configuration

After the A/B characterization, the additional $\boxed{315\,\text{pF}}$ stress capacitor is disconnected.

The final BNA therefore operates with $\boxed{C_{st,\text{final}} = 15\,\text{pF}}$ and $\boxed{C_{n,\text{final}} = 1\,\text{pF}}$.
The final compensation capacitor must satisfy

$$\boxed{C_n < \frac{R_s}{R_f} C_{st}}$$

and, using $R_s = 30\,\text{k}\Omega$, $R_f = 270\,\text{k}\Omega$, and $C_{st} = 15\,\text{pF}$,

$$\frac{30}{270}(15\,\text{pF}) = 1.67\,\text{pF}.$$

Therefore,

$$\boxed{1\,\text{pF} < 1.67\,\text{pF}}$$

confirming that the selected final compensation capacitor satisfies the neutralization condition.
Its approximate negative-capacitance contribution is

$$\boxed{C_{\text{neg,final}} \approx -9(1\,\text{pF}) = -9\,\text{pF}}$$

and hence the approximate effective residual capacitance becomes

$$\boxed{C_{\text{eff,final}} \approx 15\,\text{pF} - 9\,\text{pF} = 6\,\text{pF}}$$

Thus, after the temporary stress network is removed, the physical input capacitance returns to 15 pF, while the 1 pF active compensation capacitor reduces the approximate effective capacitive loading to 6 pF.

7 Dynamic Baseline Recovery

The second major characterization of the BNA evaluates its response to a large capacitive electrode disturbance. A controlled charge is stored on an input coupling capacitor before the electrode node is connected to the BNA.

7.1 Capacitive Disturbance Model

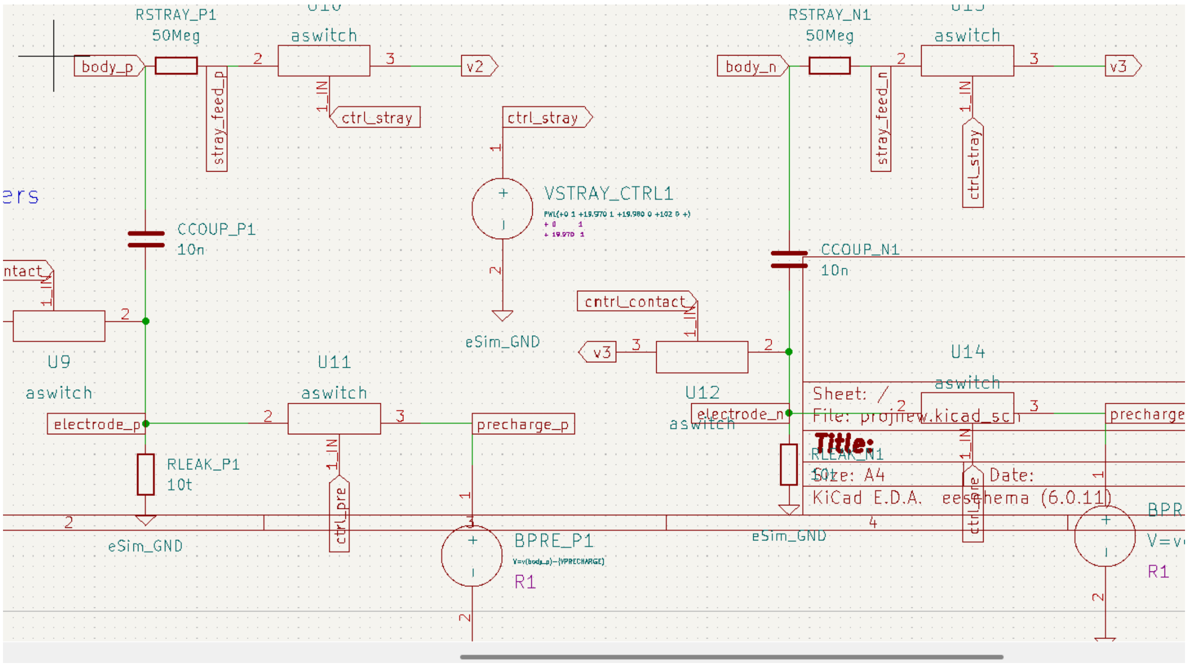

Figure 4: Controlled capacitive disturbance model used for baseline-recovery evaluation.

The recovery model uses $\boxed{C_{\mathrm{COUP}} = 10\,\mathrm{nF}}$ between each body node and its corresponding electrode node. A leakage resistance of approximately $\boxed{R_{\mathrm{LEAK}} = 10\,\mathrm{T\Omega}}$ provides a weak DC reference to the electrode node.

7.2 Structurally Symmetric Two-Channel Model

Matched Positive and Negative Input Structure

Both channels contain the same coupling and switching topology.
For the positive channel,

$$\boxed{body_p \rightarrow C_{\mathrm{COUP,P}} \rightarrow electrode_p \rightarrow v_2}$$

and for the negative channel,

$$\boxed{body_n \rightarrow C_{\mathrm{COUP,N}} \rightarrow electrode_n \rightarrow v_3}$$

The two branches therefore use the same 10 nF **coupling capacitance**, the same switching structure, and the same BNA input topology.
The hardware structure is therefore $\boxed{\textbf{structurally symmetric}}$.
The disturbance itself is intentionally asymmetric so that a differential electrode transient is created.

7.3 Controlled Precharge

[Positive-Channel Precharge]
For the positive channel, the precharge voltage is defined as

$$\boxed{V_{\mathrm{pre,P}} = V(body_p) - V_{\mathrm{PRECHARGE}}}$$

with the selected precharge magnitude $\boxed{V_{\mathrm{PRECHARGE}} = 3.2\,\mathrm{V}}$.
Therefore,

$$\boxed{V_{C,\mathrm{P}} = V(body_p) - V_{\mathrm{pre,P}} = V(body_p) - \left[V(body_p) - 3.2\right] = 3.2\,\mathrm{V}}$$

The precharge source tracks the ECG voltage itself. Consequently, the stored disturbance remains approximately 3.2 V even while the ECG waveform changes.

Negative-Channel Reference Condition
For the negative channel,

$$\boxed{V_{\mathrm{pre,N}} = V(body_n)}$$

and hence

$$\boxed{V_{C,\mathrm{N}} \approx 0\,\mathrm{V}}$$

Thus, although both channels use the same physical coupling and switching structure, the stored capacitor voltages are intentionally different:

$$\boxed{\mathbf{V}_{\mathbf{C,P}} \approx 3.2\,\mathrm{V}, \qquad \mathbf{V}_{\mathbf{C,N}} \approx 0\,\mathrm{V}}$$

This controlled asymmetry produces the differential electrode disturbance required for the baseline-recovery experiment.

[Symmetric Circuit, Asymmetric Disturbance]
Both channels contain identical coupling capacitors, leakage paths, switches, and BNA stages.
Only the initial stored voltage differs:

$$\boxed{V_{C,\mathrm{P}} \approx 3.2\,\mathrm{V}, \qquad V_{C,\mathrm{N}} \approx 0}.$$

This produces a controlled differential electrode disturbance without using different physical BNA topologies.

7.4 Recovery Switching Sequence

The precharge switch remains closed until approximately **29.99 s** so that the desired initial capacitor voltage is established.

The precharge path then opens and the electrode-contact switch closes at approximately **30.01 s**.

The stored charge is therefore applied to the BNA input as a controlled electrode transient.

7.5 Nonlinear Resistance Activation

The BNA transition occurs when $\boxed{|V_{R49}| > V_{\mathrm{THR}}}$.
With the selected threshold $\boxed{V_{\mathrm{THR}} = 2.17\,\mathrm{V}}$, the latest simulation produced a peak magnitude of $\boxed{|V_{R49}|_{\max} = 2.200\,577\,\mathrm{V}}$.
The threshold was crossed upward at $\boxed{t_{\mathrm{rise}} = 30.006\,00\,\mathrm{s}}$ and crossed downward at $\boxed{t_{\mathrm{fall}} = 37.024\,99\,\mathrm{s}}$.
Therefore, the duration for which the nonlinear resistance remained beyond the threshold region is

$$\boxed{T_{\mathrm{active}} = t_{\mathrm{fall}} - t_{\mathrm{rise}} = 37.02499 - 30.00600 = 7.018\,99\,\mathrm{s}}$$

$$T_{\mathrm{active}} = t_{\mathrm{fall}} - t_{\mathrm{rise}} \tag{25}$$

$$= 37.02499 - 30.00600 \tag{26}$$

$$= \boxed{7.018\,99\,\mathrm{s}}. \tag{27}$$

7.6 Dynamic Resistance Transition

At the threshold, $\boxed{R_{49} \approx 10\,\mathrm{M\Omega}}$.
At the peak disturbance, the measured minimum resistance is $\boxed{R_{49,\min} = 44.07\,\mathrm{k\Omega}}$.
Hence, the nonlinear resistance follows the approximate transition sequence

$$\boxed{20\,\mathrm{M\Omega} \rightarrow 10\,\mathrm{M\Omega} \rightarrow 44.1\,\mathrm{k\Omega} \rightarrow 10\,\mathrm{M\Omega} \rightarrow 20\,\mathrm{M\Omega}}$$

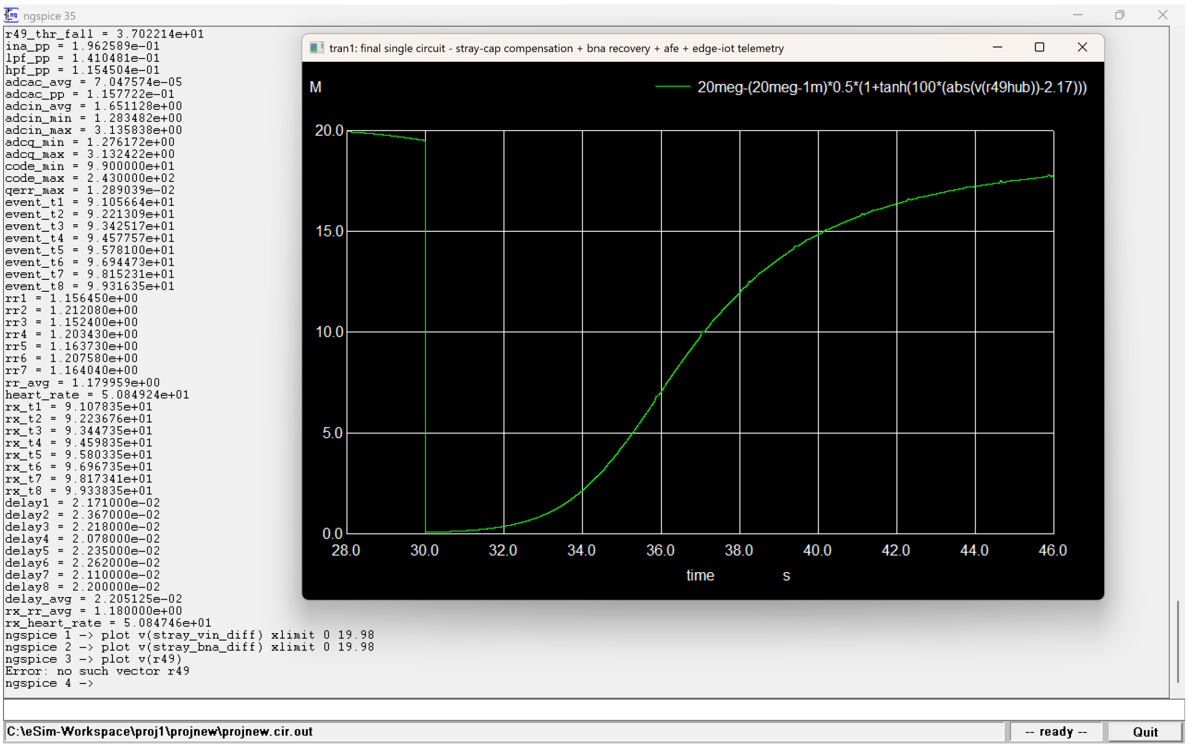

Figure 5: Dynamic change in R_{49} during the electrode disturbance.

7.7 Baseline-Recovery Criterion

The steady-state input baseline is determined from the final settled portion of the simulation.

The baseline error is defined as

$$\boxed{e_B(t) = \left|V_{\text{base}}(t) - V_{\text{base,ss}}\right|}. \tag{28}$$

Recovery is declared when the baseline error falls below

$$\boxed{e_B = 0.5\,\text{mV}}$$

for the final time.

The final crossing rather than the first crossing is used because the transient may briefly enter the 0.5 mV region before later leaving it again.

Thus,

$$\boxed{T_{\text{BR}} = t_{\text{recover,last}} - t_{\text{disturbance}}}. \tag{29}$$

7.8 Baseline-Recovery Waveform

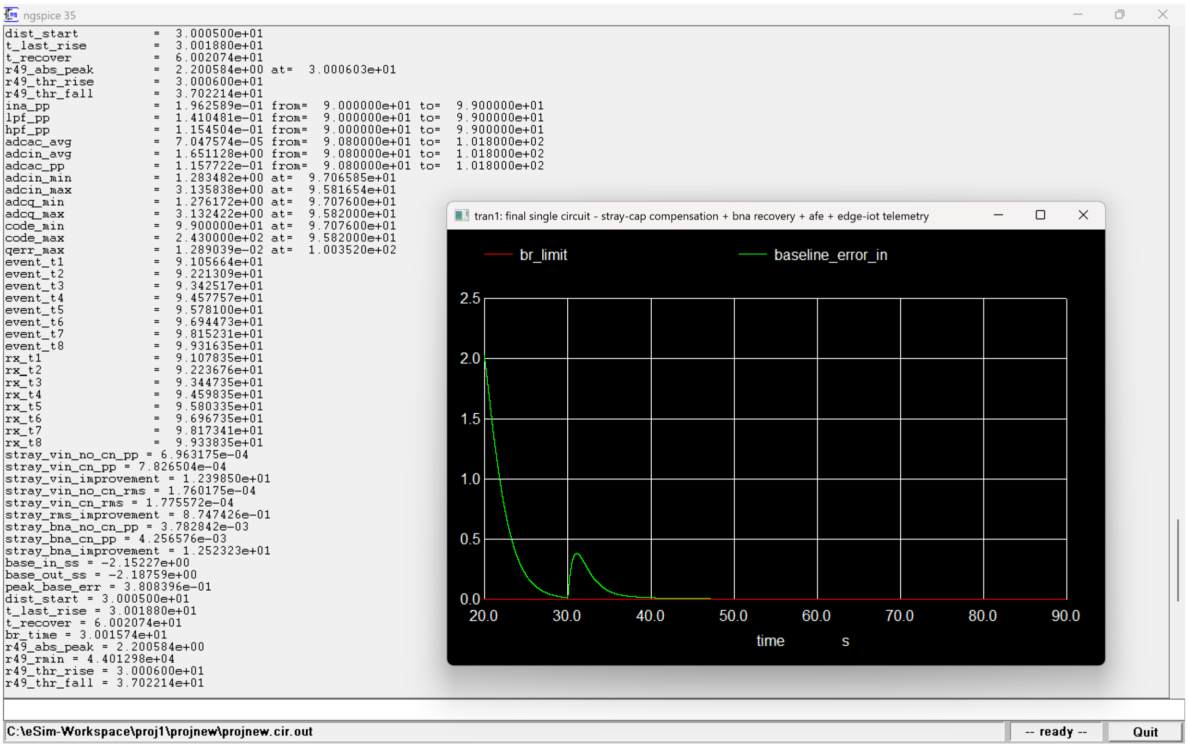

Figure 6: Baseline displacement and final recovery following the controlled electrode disturbance.

7.9 Measured Recovery Performance

The latest recovery measurements are summarized in Table 8.

Table 8: Measured dynamic BNA recovery performance.

Parameter	Measured Value
Switching threshold	2.17 V
Disturbance start	30.005 00 s
Peak baseline error	380.46 mV
Peak $\lvert V_{R49} \rvert$	2.200 577 V
Threshold entry	30.006 00 s
Threshold exit	37.024 99 s
Low-resistance active interval	7.018 99 s
Minimum R_{49}	44.07 kΩ
Final recovery time	60.079 26 s
Baseline-recovery duration	30.074 26 s

8 Instrumentation Amplifier and Analog Filtering

Following the dual BNA stage, the two conditioned input channels are converted into a single differential ECG waveform and passed through the analog filtering chain. The purpose of these stages is to increase the useful differential signal level while progressively restricting interference and out-of-band components before ADC interfacing.

The analog chain is

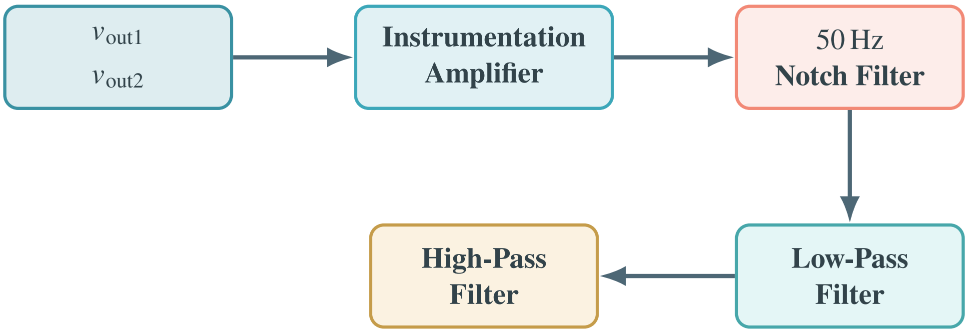

Figure 7: Analog signal progression from the BNA outputs through differential amplification and filtering.

8.1 Instrumentation Amplifier

The outputs of the two BNA channels are applied to a discrete instrumentation-amplifier stage constructed using OPA827 operational amplifiers. The stage converts the differential BNA signal into a single-ended amplified ECG while suppressing components that are common to both input channels.

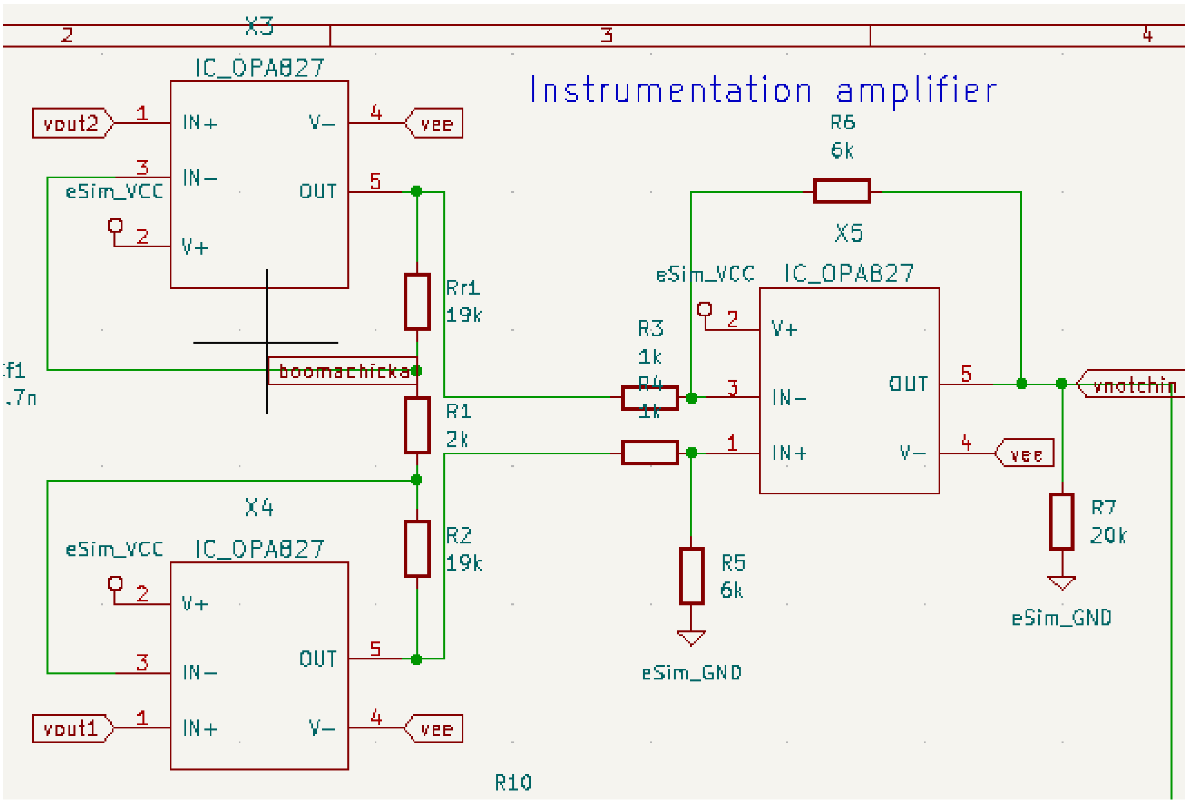

Figure 8: Discrete OPA827 instrumentation-amplifier stage following the BNA.

The principal resistance values used in the differential amplifier are summarized below.

The principal instrumentation-amplifier component values are $R_1 = 2\,\mathrm{k\Omega}$, $R_2 = R_{r1} = 19\,\mathrm{k\Omega}$, $R_3 = R_4 = 1\,\mathrm{k\Omega}$, and $R_5 = R_6 = 7.5\,\mathrm{k\Omega}$. Matched resistance values are important in the differential section because mismatch directly degrades common-mode cancellation.

Differential Signal Formation

The BNA produces two simultaneously conditioned signals. The instrumentation stage responds primarily to their difference,

$$\boxed{V_{\mathrm{diff}} = V(v_{\mathrm{out1}}) - V(v_{\mathrm{out2}})}$$

and converts this quantity into a single-ended ECG waveform for subsequent filtering.

```
dist_start = 3.000500e+01
t_last_rise = 3.001880e+01
t_recover = 6.002074e+01
br_time = 3.001574e+01
r49_abs_peak = 2.200584e+00
r49_rmin = 4.401298e+04
r49_thr_rise = 3.000600e+01
r49_thr_fall = 3.702214e+01
ina_pp = 1.962589e-01
lpf_pp = 1.410481e-01
hpf_pp = 1.154504e-01
adcac_avg = 7.047574e-05
adcac_pp = 1.157722e-01
adcin_avg = 1.651128e+00
adcin_min = 1.283482e+00
adcin_max = 3.135838e+00
adcq_min = 1.276172e+00
adcq_max = 3.132422e+00
code_min = 9.900000e+01
code_max = 2.430000e+02
qerr_max = 1.289039e-02
event_t1 = 9.105664e+01
event_t2 = 9.221309e+01
event_t3 = 9.342517e+01
event_t4 = 9.457757e+01
event_t5 = 9.578100e+01
event_t6 = 9.694473e+01
event_t7 = 9.815231e+01
event_t8 = 9.931635e+01
```

Figure 9: Transient ECG waveform at the instrumentation-amplifier output.

Instrumentation-Amplifier Output

$$\boxed{V_{\mathrm{INA,pp}} = 196.25\,\mathrm{mV}}$$

The differential ECG is therefore raised to a substantially larger voltage level before entering the analog filter chain.

8.2 50 Hz Notch Filter

The instrumentation-amplifier output is applied to a notch network designed around the mains-interference region. The principal component values are $R_8 = R_{10} = 3.3\,\mathrm{k\Omega}$, $R_9 = 300\,\mathrm{k\Omega}$, $C_1 = C_3 = 100\,\mathrm{nF}$, and $C_2 = 200\,\mathrm{nF}$.

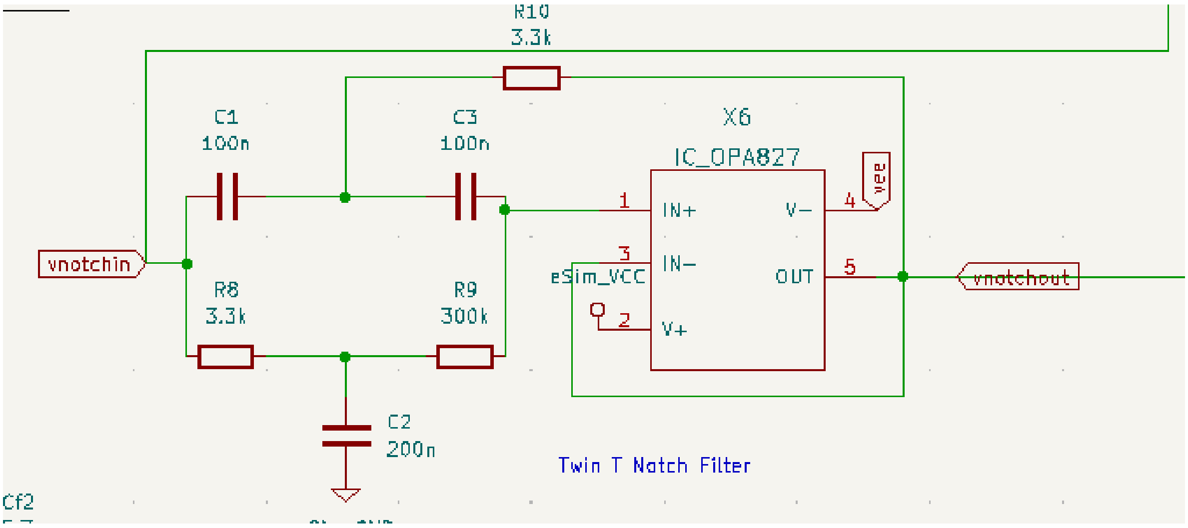

Figure 10: 50 Hz interference-suppression stage.

8.3 Low-Pass Filter

Low-Pass Filter Stage

The notch-filter output is followed by an active low-pass stage using $R_{11} = R_{12} = 22\,\mathrm{k\Omega}$ and $C_4 = C_5 = 47\,\mathrm{nF}$.
The purpose of this stage is to restrict excessive high-frequency content before the signal reaches the final high-pass stage and ADC interface.

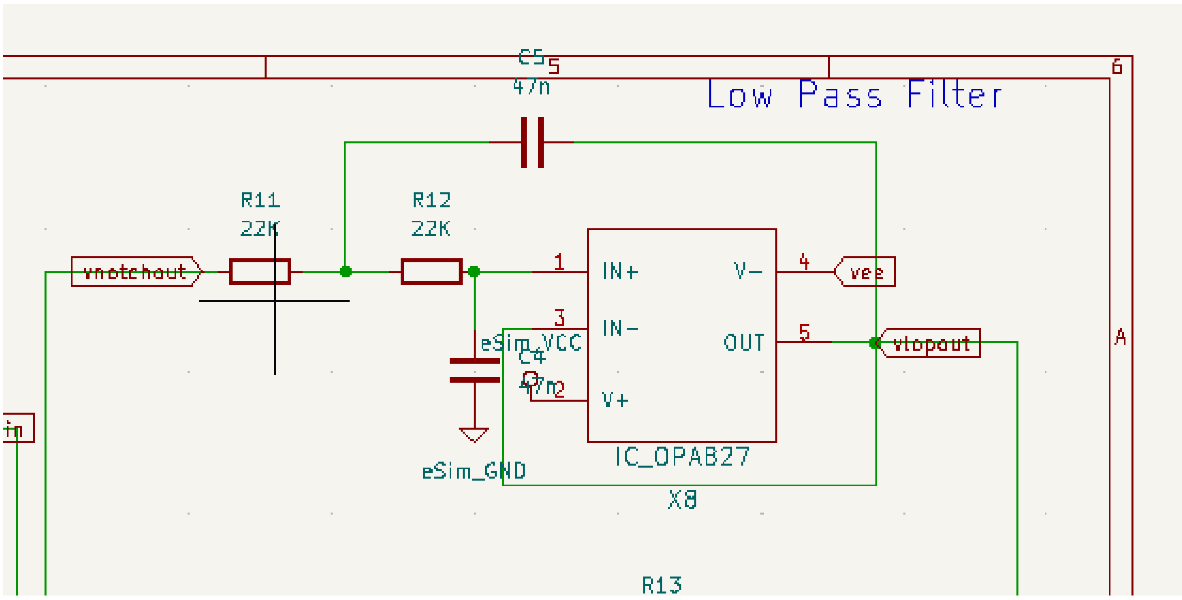

Figure 11: Active low-pass filtering stage.

The measured steady-state output was

Low-Pass Output

$$\boxed{V_{\mathrm{LPF,pp}} = 141\ \mathrm{mV}}$$

8.4 High-Pass Filter

High-Pass Filter Stage

Very-low-frequency baseline content is further reduced using the final high-pass stage. Its principal values are

$$\boxed{\mathbf{R_{13}} = \mathbf{R_{14}} = 15\,\mathrm{k\Omega}}$$

and

$$\boxed{\mathbf{C_6} = \mathbf{C_7} = 33\,\mu\mathrm{F}}$$

These values define the final low-frequency conditioning stage before the signal is passed to the ADC interface.

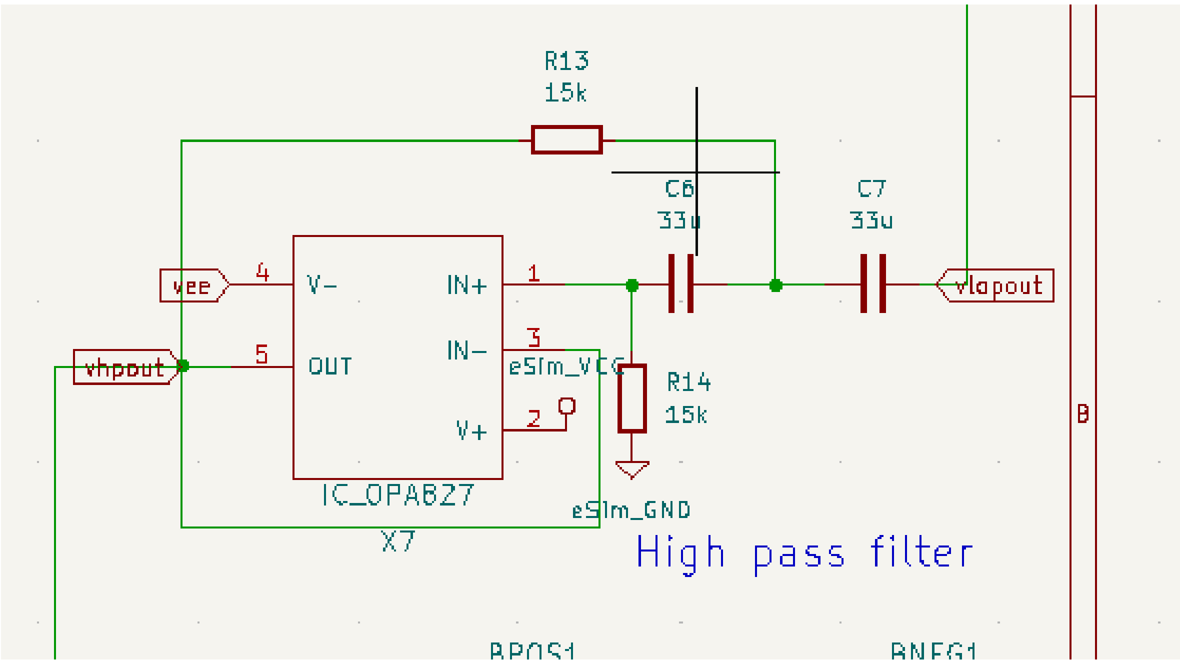

Figure 12: Final high-pass filtering stage of the analog front-end.

The measured final analog AFE output was

Final Analog AFE Output

$$\boxed{V_{\mathrm{HPF,pp}} = 115.4\,\mathrm{mV}}$$

This node, v_{hpout}, is the final analog waveform delivered to the ADC-conditioning stage.

8.5 Analog-Stage Performance Summary

Table 9: Measured steady-state analog signal levels.

Stage	Peak-to-Peak Output
Instrumentation amplifier	196.13 mV
Low-pass filter	140.96 mV
High-pass filter	115.36 mV

Analog-Chain Interpretation

The instrumentation stage converts and amplifies the differential BNA output, after which the analog filtering stages progressively condition the waveform.
The final analog output remains clearly resolved at approximately

$$\boxed{115.36\,\mathrm{mV}_{pp}}$$

and is subsequently AC-coupled and rebias-conditioned for operation within the 0 V to 3.3 V ADC input range.

9 Total Circuit

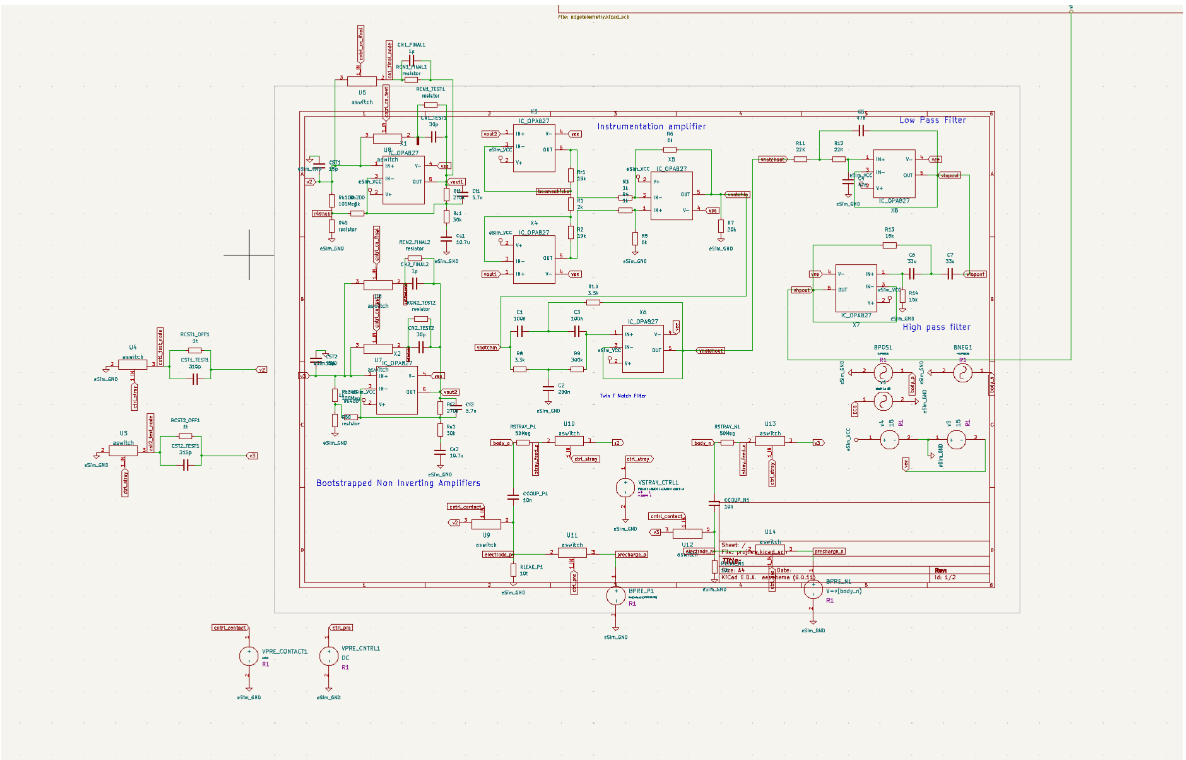

Figure 13: Entire ECG circuit

10 ADC Interface and 8-Bit Digitization

The final analog ECG at v_{hpout} is AC-coupled, amplified, shifted to the midpoint of a 0 V to 3.3 V range, sampled, and finally represented by an 8-bit quantizer.

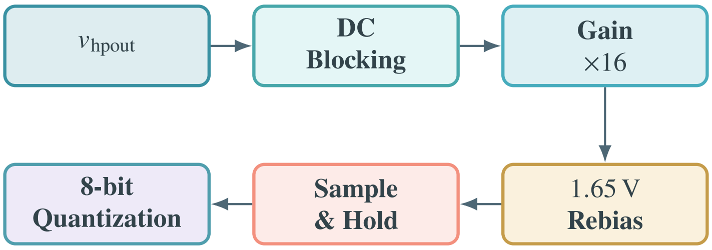

Figure 14: ADC conditioning and digitization sequence.

10.1 DC Removal and ADC Scaling

The ADC interface uses $\boxed{C_{\text{ADC}} = 1\,\mu\text{F}}$ and $\boxed{R_{\text{ADC}} = 3.3\,\text{M}\Omega}$ to remove the residual DC level from v_{hpout}. The resulting corner frequency is $\boxed{f_c \approx 0.048\,\text{Hz}}$, which lies well below the useful ECG band. The zero-centered signal is then amplified by $\boxed{A = 16}$ and shifted by $\boxed{V_{\text{BIAS}} = 1.65\,\text{V}}$, giving

$$\boxed{V_{\text{ADC,in}} = 1.65 + 16V_{\text{ADC,ac}}}$$

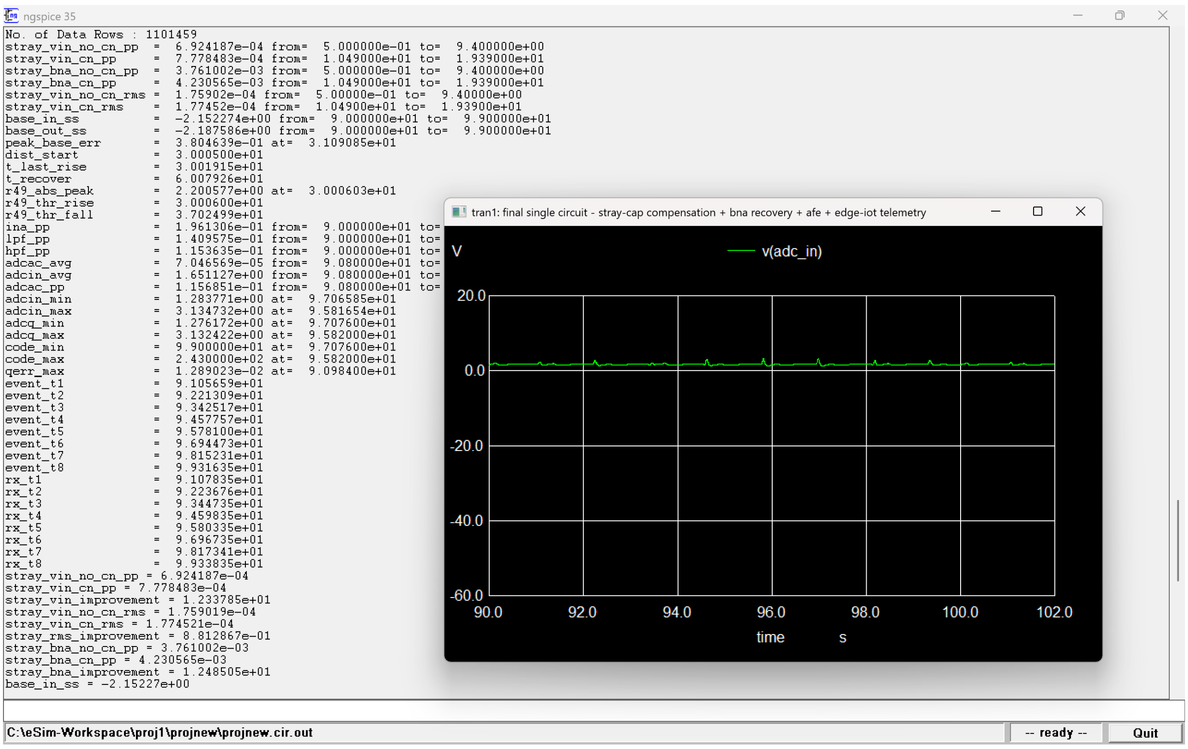

Figure 15: Progression from the final analog ECG to the rebias-conditioned ADC input.

10.2 Sampling and Hold

Sampling Configuration

The sampling clock has a period of $\boxed{T_s = 4\,\mathrm{ms}}$, corresponding to

$$\boxed{f_s = \frac{1}{T_s} = 250\,\mathrm{S/s}}$$

The sampling switch stores each instantaneous ADC-input value on $\boxed{C_H = 1\,\mathrm{nF}}$. A very large $\boxed{R_H = 1\,\mathrm{T\Omega}}$ provides a weak DC reference without materially discharging the held sample.

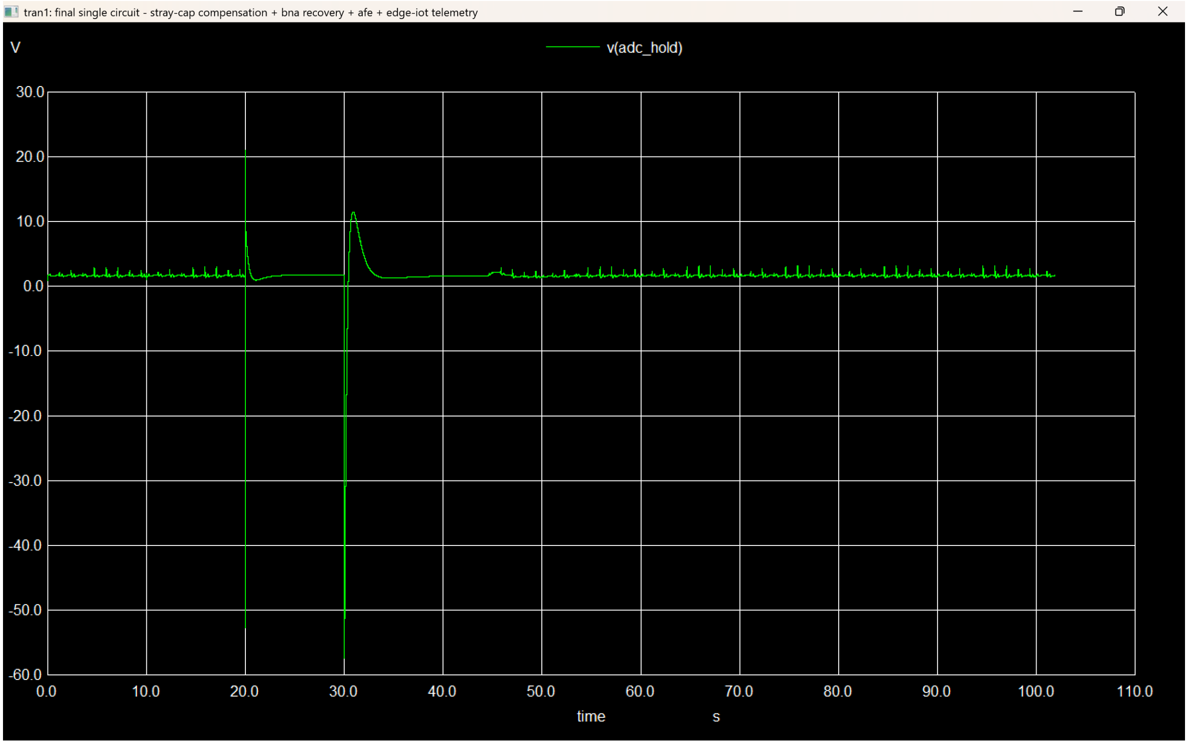

Figure 16: ADC hold waveform at 250 S/s.

10.3 8-Bit Quantization

Quantizer Resolution

For a 0 V to 3.3 V, 8-bit conversion range, the voltage represented by one digital step is

$$\boxed{V_{\mathrm{LSB}} = \frac{3.3\,\mathrm{V}}{256} = 12.890\,625\,\mathrm{mV}}$$

The implemented model therefore evaluates

$$V_Q = \left\lfloor \frac{V_{\mathrm{hold}}}{V_{\mathrm{LSB}}} \right\rfloor V_{\mathrm{LSB}}.$$

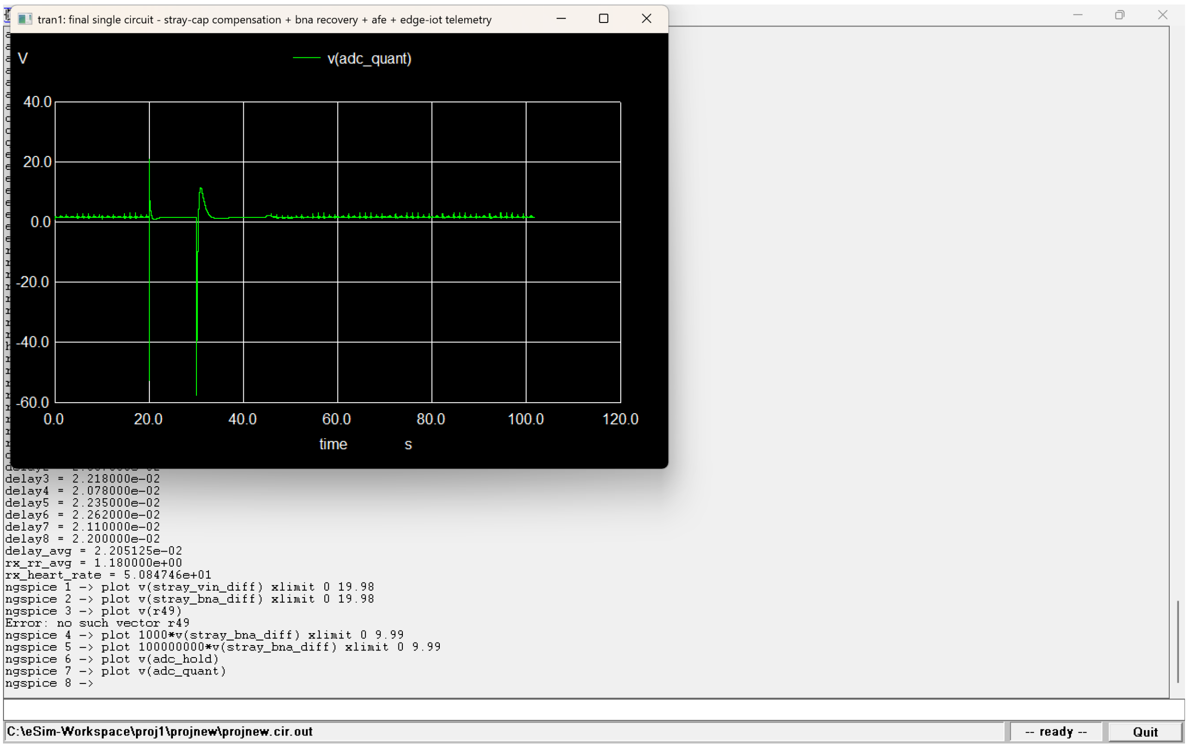

Figure 17: Sampled ECG and corresponding 8-bit quantized representation.

10.4 ADC Performance

Measured ADC Performance

The conditioned ADC input had a mean value of 1.651 13 V and remained between 1.283 77 V and 3.134 73 V.

The resulting 8-bit codes occupied the range 99–243, while the maximum measured quantization error was 12.890 23 mV.

This is effectively one ideal ADC least-significant bit.

11 QRS and Edge-Event Extraction

Rather than transmitting the complete digitized ECG waveform, the subsequent circuit extracts individual cardiac events from the quantized signal. This reduces the downstream information to compact edge-triggered event pulses.

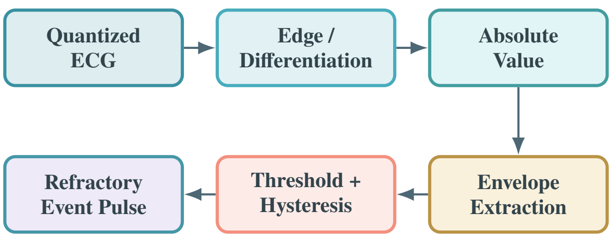

Figure 18: Edge-based QRS-event extraction sequence.

11.1 Edge Enhancement and Envelope Formation

QRS Preprocessing

The quantized ADC signal is first re-centered by subtracting $\boxed{1.65\,\mathrm{V}}$.

QRS transitions are emphasized using $\boxed{C_{\mathrm{QRS}} = 100\,\mathrm{nF}}$ and $\boxed{R_{\mathrm{QRS}} = 10\,\mathrm{k\Omega}}$, after which the absolute magnitude is formed.

The rectified signal is smoothed by an envelope network using $\boxed{R_{\mathrm{ENV}} = 100\,\mathrm{k\Omega}}$ and $\boxed{C_{\mathrm{ENV}} = 100\,\mathrm{nF}}$.

Figure 19: QRS-envelope formation.

11.2 Threshold Detection and Refractory Control

QRS detection uses a Schmitt-trigger switch with $\boxed{V_T = 8\,\mathrm{mV}}$ and $\boxed{V_H = 1.6\,\mathrm{mV}}$.
The control signal also includes refractory feedback,

$$\boxed{V_{\mathrm{QRS,ctrl}} = V_{\mathrm{env}} - 0.05V_{\mathrm{refractory}}}$$

so that a recently detected event temporarily suppresses immediate retriggering.
A rising QRS transition is converted into a positive edge using $\boxed{C_{\mathrm{edge}} = 100\,\mathrm{nF}}$ and $\boxed{R_{\mathrm{edge}} = 100\,\mathrm{k\Omega}}$.

11.3 Event-Pulse Generation

Trigger and Refractory Timing

The edge pulse charges a trigger-hold network formed by $\boxed{C_{\text{TRIG}} = 100\,\text{nF}}$ and $\boxed{R_{\text{TRIG}} = 220\,\text{k}\Omega}$.

A second monostable establishes the refractory interval using $\boxed{C_{\text{REF}} = 100\,\text{nF}}$ and $\boxed{R_{\text{REF}} = 3.3\,\text{M}\Omega}$.

The final event node is generated from the refractory voltage around the $\boxed{0.70\,\text{V}}$ decision level.

11.4 Heart-Rate Estimation

Detected Cardiac Events

The final evaluation interval produced **8 detected events**.

The measured mean R–R interval was $\boxed{1.179\,97\,\text{s}}$, giving

$$\boxed{HR = \frac{60}{RR_{\text{avg}}} = 50.85\,\text{bpm}}$$

More precisely, the measured value was $\boxed{50.848\,94\,\text{bpm}}$.

12 Event-Driven OOK Telemetry

The extracted cardiac-event pulse is transmitted rather than the entire ECG waveform. A simple on–off-keying (OOK) stage therefore provides a compact proof-of-concept telemetry link.

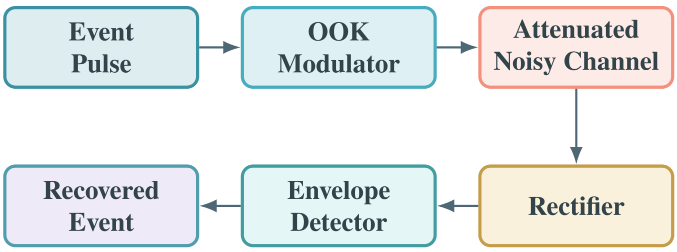

Figure 20: Event-driven OOK telemetry and receiver chain.

12.1 OOK Transmission

The event pulse gates a sinusoidal carrier at $\boxed{f_c = 100\,\text{Hz}}$, producing

$$\boxed{V_{\text{TX}} = V_{\text{event}} V_{\text{carrier}}}$$

Only detected cardiac events therefore activate the transmitted carrier.

12.2 Channel Model

Attenuated and Noisy Channel

The telemetry channel applies an amplitude factor of $\boxed{0.35}$ to the transmitted waveform and adds sinusoidal interference with $\boxed{A_N = 30\,\text{mV}}$ at $\boxed{f_N = 23\,\text{Hz}}$.
Thus,

$$\boxed{V_{\text{RX,raw}} = 0.35V_{\text{TX}} + V_{\text{noise}}}$$

12.3 Envelope Detection and Event Recovery

Receiver Configuration

The received waveform is full-wave rectified and passed through an envelope detector using $\boxed{R_{\text{DET}} = 10\,\text{k}\Omega}$ and $\boxed{C_{\text{DET}} = 2.2\,\mu\text{F}}$.
The reconstructed event is generated with a Schmitt threshold of $\boxed{V_T = 0.12\,\text{V}}$ and hysteresis $\boxed{V_H = 0.03\,\text{V}}$.

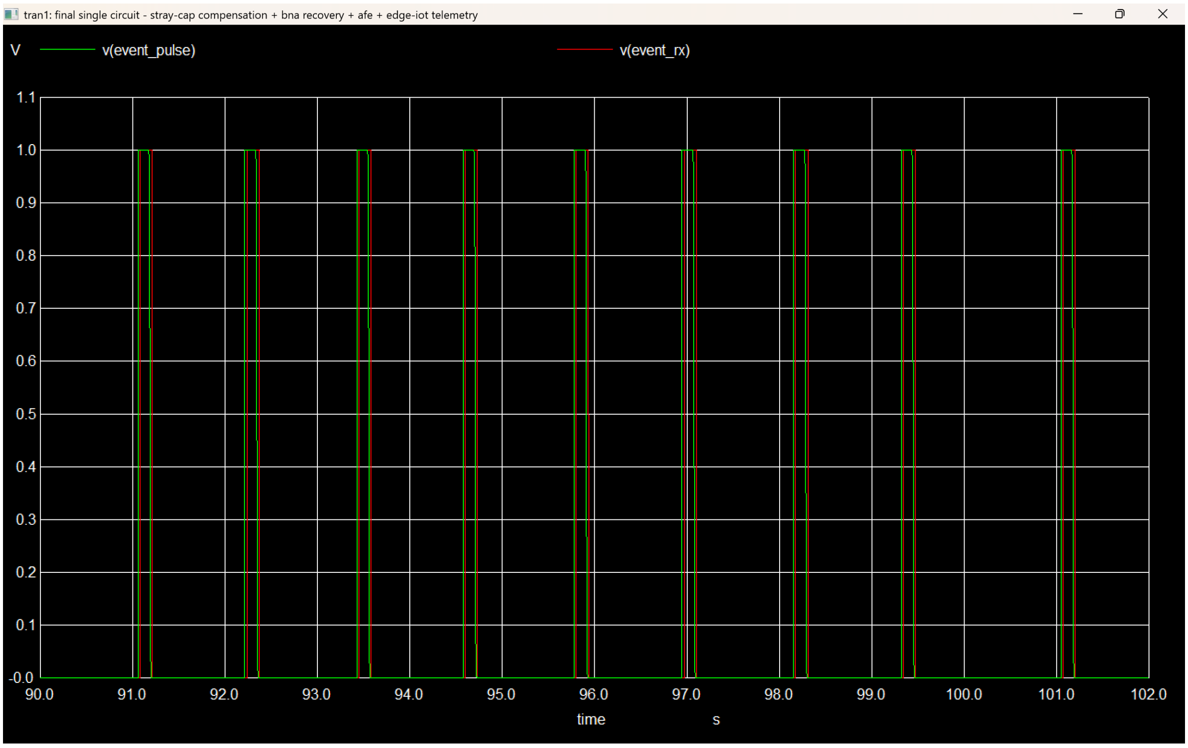

Figure 21: event pulse and event rx

12.4 Telemetry Performance

End-to-End Event Recovery

All **8 transmitted events** were recovered at the receiver, giving an event-recovery result of **8/8**.

The average transmitter-to-receiver event delay was 22.06 ms.

The received R–R interval was 1.180 00 s, corresponding to a recovered heart rate of 50.847 46 bpm.

Integrated Digital-Backend Result

The complete backend therefore performs

Analog ECG → 8-bit ADC → QRS Event → OOK Transmission → Recovered Event

while preserving all eight detected cardiac events across the simulated attenuated and noisy communication channel.

13 Discussion

13.1 Relation to the Reference AFE

Reference Architecture

The input-stage concept implemented in this work is based on the analogue front-end proposed by **Hajime Nakamura, Yuichiro Sakajiri, Hiroshi Ishigami, and Akinori Ueno** in their work entitled *"A Novel Analog Front End with Voltage-Dependent Input Impedance and Bandpass Amplification for Capacitive Biopotential Measurements"*.

Their AFE combines three principal ideas: **voltage-dependent input impedance**, **bandpass amplification**, and **stray-capacitance reduction**.

The present work adapts these principles into a complete eSim/ngspice ECG acquisition chain and extends the circuit-level study through ADC interfacing, QRS-event extraction, and event-driven telemetry.

13.2 Adaptive Input-Impedance Behaviour

During ordinary ECG acquisition, the nonlinear BNA resistance remains near 20 MΩ, maintaining a high-input-impedance condition.

When the disturbance magnitude exceeds $V_{\mathrm{THR}} = 2.17\,\mathrm{V}$, the nonlinear resistance decreases sharply and reached a simulated minimum of $R_{49,\mathrm{min}} = 44.07\,\mathrm{k\Omega}$.

The input stage therefore exhibits the intended adaptive behaviour:

high-impedance acquisition → disturbance → temporary low resistance → high impedance restored

This behaviour addresses the fundamental sensitivity–stability trade-off described by Nakamura *et al.*: a high input impedance benefits weak capacitive biopotential acquisition, whereas a lower effective impedance during large disturbances enables faster discharge of accumulated charge.

13.3 Effect of Stray-Capacitance Neutralization

Capacitive-Loading Reduction

The permanent input parasitic capacitance of the final BNA is $C_{st} = 15\,\mathrm{pF}$.

For characterization, an additional 315 pF was temporarily introduced, producing a total stress capacitance of 330 pF.

With $C_n = 30\,\mathrm{pF}$, the BNA produces an approximate effective negative-capacitance contribution of

$$\boxed{C_{\mathrm{neg}} \approx -\frac{R_f}{R_s} C_n = -270\,\mathrm{pF}}$$

and therefore an approximate residual loading of

$$\boxed{C_{\mathrm{eff}} \approx 330 - 270 = 60\,\mathrm{pF}}.$$

The measured differential ECG peak-to-peak amplitude increased by **12.34%** at the input and **12.49%** at the BNA output.
The physical 330 pF capacitance remains connected during the compensated stress interval; the reduction to approximately 60 pF refers to the *effective* capacitive loading produced by active neutralization.

13.4 Dynamic Baseline-Recovery Behaviour

Recovery Response

The controlled recovery experiment used $C_{\mathrm{COUP}} = 10\,\mathrm{nF}$ with a positive-channel precharge of 3.2 V.

Following electrode contact, the nonlinear resistance entered its low-resistance region at 30.006 00 s and left the threshold region at 37.024 99 s, giving an active nonlinear interval of 7.018 99 s.

The final baseline-recovery duration, evaluated using the final 0.5 mV error crossing, was 30.074 26 s.

The nonlinear active interval and the total baseline-recovery time are not the same quantity. Once the input voltage falls below the nonlinear threshold, R_{49} returns toward its high-resistance state, but the remaining low-amplitude baseline component continues settling through the high-impedance network.

Consequently, the final recovery criterion is intentionally based on the **last** threshold crossing rather than the first temporary crossing.

13.5 Use of Recorded ECG Data

PTB-XL Input Signal

The ECG input used for transient verification was obtained from the **PTB-XL** database developed and published by **Patrick Wagner, Nils Strodthoff, Ralf-Dieter Bousseljot, Dieter Kreiseler, Fatima I. Lunze, Wojciech Samek, and Tobias Schaeffter**.

The selected waveform was taken from record `12002_lr` using **Lead I**.
The recorded ECG was converted to a piecewise-linear source for ngspice so that the complete analog and digital signal chain could be tested with realistic ECG morphology rather than an artificial sinusoidal input.

13.6 Analog Conditioning and Digitization

The final analog chain produced $196.13\,\mathrm{mV}_{pp}$ at the instrumentation-amplifier output, $140.96\,\mathrm{mV}_{pp}$ after low-pass filtering, and $115.36\,\mathrm{mV}_{pp}$ at the final high-pass output.
Instead of subtracting a fixed simulated DC offset, the final ADC interface uses physical AC coupling through $C_{\mathrm{ADC}} = 1\,\mu\mathrm{F}$ and $R_{\mathrm{ADC}} = 3.3\,\mathrm{M}\Omega$.
The resulting ECG is amplified by 16 and biased at 1.65 V before 8-bit conversion.
The conditioned ADC input remained within 1.283 77 V to 3.134 73 V, avoiding both conversion rails.

13.7 Event-Based Processing and Telemetry

Edge-IoT Backend

The digitized ECG is reduced to discrete QRS-event pulses rather than transmitting the complete waveform. A total of **8 events** were detected, with an average R–R interval of 1.179 97 s and a calculated heart rate of 50.848 94 bpm.
The extracted events were transmitted using a 100 Hz OOK carrier through a channel containing an amplitude factor of 0.35 and 30 mV of 23 Hz sinusoidal interference.
All **8/8 events** were recovered, with an average receiver delay of 22.06 ms.

13.8 Scope and Limitations

The present work is a circuit-level simulation and does not constitute clinical validation of the AFE.
The 330 pF stray-capacitance configuration is an intentional stress condition used to demonstrate capacitive neutralization. The final input model retains only 15 pF of permanent stray capacitance.
Similarly, the 3.2 V precharge stimulus is a controlled disturbance used specifically for baseline-recovery characterization.
The QRS and OOK stages are behavioural circuit-level demonstrations and are not intended to replace clinical ECG-analysis algorithms or a complete practical radio-frequency communication system.

14 Conclusion

14.1 Conclusion

Overall Outcome

An integrated ECG analog front-end and event-telemetry system was designed and verified using eSim and ngspice.
The input architecture was developed from the voltage-dependent-impedance, bandpass-amplification, and stray-capacitance-reduction principles reported by **Hajime Nakamura, Yuichiro Sakajiri, Hiroshi Ishigami, and Akinori Ueno**.
The resulting dual BNA stage maintained a high-resistance input state during normal acquisition while reducing R_{49} to approximately 44.07 kΩ during the controlled disturbance.

Capacitive neutralization produced measured differential amplitude improvements of **12.34%** at the BNA input and **12.49%** at the BNA output.

The baseline-recovery experiment produced a final recovery duration of 30.07 s.

The complete analog chain generated a final conditioned ECG of $115.36\,\mathrm{mV}_{pp}$, which was AC-coupled, amplified, rebias-conditioned, sampled at 250 S/s, and quantized using an **8-bit** ADC model.
Using the PTB-XL ECG waveform published by **Patrick Wagner and co-authors**, the digital back-end detected **8 cardiac events**, estimated a heart rate of approximately 50.85 bpm, and recovered **8/8 transmitted events** after the simulated OOK telemetry channel.
The complete simulation therefore demonstrates a single integrated path from high-input-impedance ECG acquisition through adaptive disturbance recovery, analog conditioning, digitization, event detection, and event-level telemetry.

15 References

References

[1] H. Nakamura, Y. Sakajiri, H. Ishigami, and A. Ueno, "A Novel Analog Front End with Voltage-Dependent Input Impedance and Bandpass Amplification for Capacitive Biopotential Measurements," *Sensors*, vol. 20, no. 9, Art. no. 2476, 2020. doi: 10.3390/s20092476.

[2] P. Wagner, N. Strodthoff, R.-D. Bousseljot, D. Kreiseler, F. I. Lunze, W. Samek, and T. Schaeffter, "PTB-XL, a large publicly available electrocardiography dataset," *Scientific Data*, vol. 7, Art. no. 154, 2020. doi: 10.1038/s41597-020-0495-6.

[3] P. Wagner, N. Strodthoff, R.-D. Bousseljot, W. Samek, and T. Schaeffter, *PTB-XL, a Large Publicly Available Electrocardiography Dataset*, PhysioNet, 2020.

[4] Texas Instruments, *OPA827 Low-Noise, High-Precision, JFET-Input Operational Amplifier*, OPA827 Data Sheet, Texas Instruments.

[5] FOSSEE Team, Indian Institute of Technology Bombay, *eSim: Electronic Circuit Simulation — An Open-Source EDA Tool for Circuit Design, Simulation, Analysis and PCB Design*, FOSSEE, IIT Bombay.

[6] H. Vogt, M. Hendrix, and P. Nenzi, *Ngspice User's Manual*, Ngspice open-source circuit simulator documentation.